Measurement of fundamental nuclear decay data using Metallic Magnetic Calorimeters

FINAL PUBLISHABLE REPORT

Grant Agreement number	17FUN02
Project short name	MetroMMC
Project full title	Measurement of fundamental nuclear decay data using metallic magnetic calorimeters

Project start date and duration:		June 2018, 36 months + 6 months
Coordinator: Dirk Arnold, PTB	Tel: +49 531 592 6100	E-mail: dirk.arnold@ptb.de
Project website address: http://empir.npl.co.uk/metrommc/		
Internal Funded Partners: 1 PTB, Germany 2 CEA, France 3 NPL, United Kingdom	External Funded Partners: 4 CNRS, France 5 UHEI, Germany 6 UNL, Portugal	Unfunded Partners: 7 KRISS, Republic of Korea
RMG: -		

TABLE OF CONTENTS

1 Overview

The overall objective of this project was the improvement of the knowledge of electron capture (EC) decay and subsequent atomic relaxation processes. New theoretical calculation techniques and extensive experiments using specially adapted metallic magnetic calorimeters (MMCs) were developed to determine important decay data which are relevant when studying the influence of EC decay in cancer therapy on the DNA level or the early history of the solar system as well as for primary activity standardisations in radionuclide metrology. The experimental parts were complemented with a new approach based on microwave coupled resonators (MCRs).

All objectives have been fulfilled and new and improved theoretical models describing electron capture decay spectra have been developed. Being validated against experimental data from this project and from literature, the data from these models can be used in applications that depend on electron capture decay, such as radionuclide metrology, low background experiments, or radiometric dating, just to name a few.

2 Need

Determining the age of the solar system or how cancer treatments damage DNA are two research areas that both rely on very precise knowledge of nuclear decay probabilities related to radioactive EC decay. Atomic data for EC decays have been derived from measurements and calculations performed more than 20 years ago, and these are now causing significant measurement problems. Compiled data, for example, were based on the frozen core approximation with no explicit description of multiple ionisation processes. Therefore, accurate experimental X-ray emission intensities were needed to establish consistent EC decay schemes and theoretical models of subsequent relaxation processes.

The precise knowledge of EC probabilities is pivotal when calculating the electron and photon emissions resulting from EC decay. The accurate knowledge of these emission spectra is a prerequisite for state-of-the-art liquid scintillation counting (LSC) techniques which are frequently used for primary activity determination in radionuclide metrology. The uncertainties of fractional EC probabilities define the resulting uncertainty of the activity determined by LSC, e.g., the triple-to-double coincidence ratio (TDCR) method. A sound improvement of the quality of LSC measurements therefore required improved computation methods of emission spectra which, in turn, could only be developed based on new theoretical approaches and experimentally determined EC probabilities of the highest achievable accuracy. In addition, X-ray emission intensities are key data used to quantify the activity of a radioactive material by X-ray spectrometry.

Some of the technical developments were carried out within the EMPIR project 15SIB10 MetroBeta for pure beta-emitting isotopes with endpoint energies in the range from 70 keV to 700 keV. To study EC decays and X-ray emissions, new developments for MMC-based techniques were carried out for high precision measurements with sources both embedded in the MMC absorber and external to the detector.

3 Objectives

The overall objective of this project was the improvement of the knowledge of electron capture (EC) decay and subsequent atomic relaxation processes. The specific objectives of the project were:

1. To improve experimental techniques for spectrometry using novel cryogenic detectors based on MMCs and MCRs for radionuclide metrology in the energy range of 20 eV - 100 keV.
2. To determine fractional EC probabilities of selected radionuclides by means of spectrometry based on novel cryogenic detectors with high energy resolution and very low energy threshold using sources embedded in the detector absorber.
3. To measure absolute X-ray emission intensities of selected radionuclides by using a combination of high-resolution spectrometry based on novel cryogenic detectors using external sources and accurate primary activity determination.
4. To improve theoretical models and *ab initio* calculations of the EC process and subsequent atomic relaxation and to validate them with the high-precision experimental data from this project.

5. To facilitate the take-up of the technology and measurement infrastructure developed in the project by radionuclide metrologists, nuclear physicists and other researchers.

4 Results

Experimental techniques for spectrometry based on novel cryogenic detectors for radionuclide metrology in the energy range of 20 eV – 100 keV

Within the project *MetroMMC* the consortium partners have extended or newly developed detector technologies that enable high-resolution decay spectrometry of radionuclides decaying via electron capture (EC). Two types of Metallic Magnetic Calorimeter (MMC) detectors have been conceptualised, designed and microfabricated by UHEI. MMC detectors are energy dispersive low-temperature (< 0.1 K) detectors offering the potential to measure radionuclide decay spectra, in particular of low to medium energy transitions, with unprecedented precision. Within *MetroMMC* the MMC detectors used Er in Ag (Ag:Er) as the paramagnetic sensor material.

The first MMC detector type was optimised for decay spectrometry of electron capture (EC) radionuclides embedded inside the absorber and emitting X-rays and Auger electrons in the energy range between 20 eV and 100 keV. Here, the starting point were the heat capacities of suitable gold absorber elements, the dimensions of which were defined by radiation transport simulations at CEA and PTB. In addition, the thermodynamic properties of the Ag:Er sensor material, verified detector noise models as well as several other detector parameters being a-priori fixed according to constraints set by fabrication technology at UHEI and the available cryogenic systems at CEA and PTB entered. The achievable energy resolution for several detector configurations was calculated for varying by sensor area, sensor height, doping concentration of the paramagnet as well as the persistent current creating the required bias magnetic field. This procedure allowed to define an optimal detector design for the radionuclide of interest. As a result, five different MMC detector variants that cover an absorber heat capacity range (at a detector operating temperature of 20 mK) between 8 pJ/K and 1.7 nJ/K have been designed.

Table 1: Overview of detector parameters based on absorber dimensions.

MMC detector type	XS	S	M	L	XL
absorber heat capactity	8 pJ/K	28 pJ/K	110 pJ/K	400 pJ/K	1.7 nJ/K
sensor heat capacity	7.6 pJ/K	17.9 pJ/K	50.6 pJ/K	308 pJ/K	1.17 nJ/K
detector area	$(249\ \mu m)^2$	$(335\ \mu m)^2$	$(538\ \mu m)^2$	$(1427\ \mu m)^2$	$(2663\ \mu m)^2$
single detector inductance	3.4 nH	3.1 nH	8.0 nH	56 nH	196 nH

The chip layout of the 5 detector variants of the first MMC detector type took into consideration the technological processes available at UHEI as well as the chip layout of the PTB SQUID current sensor used for the MMC readout and, in addition, the processes at CEA and PTB to combine source/absorber elements at MMC detectors. All chips feature large on-chip heat bath (HB) to thermally couple the MMC to the base temperature. The ratio between length and cross-section of the MMC-HB link is matched to the target decay time of the detectors. In contrast to previous detectors purpose-built for high-resolution spectrometry of beta emitting radioisotopes, both temperature sensors were connected to a common on-chip heat bath to minimise temperature gradients between the sensors that potentially degrade the energy resolution. Moreover, this minimises the number of electrical contacts (bonding wires) from the actual cryogenic platform to the on-chip heat bath. Since the detector module might be different for each research group using these detectors, it is preferable to provide not only one but two or three different interface configurations (pads for electrical connections via bonding wires) that allow connecting the detector. For this reason, three sets of electrical contact pads located at the left, lower and right side of the detector chip are used. These are routed to a common summing point such that the detector performance is not affected by the choice of the set of contact pads.

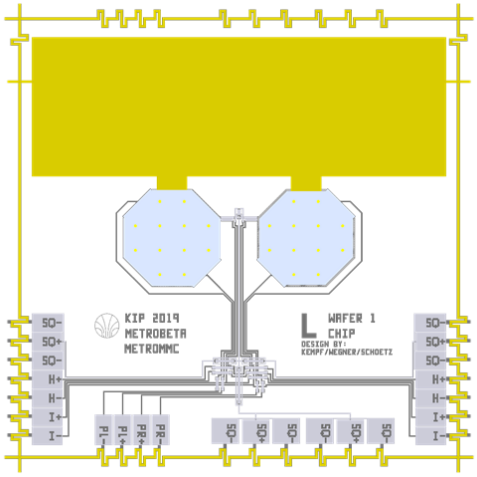

Figure 1: Design drawing of one of the designed and fabricated detectors (type "L") for EC spectrometry. The yellow box at the upper edge of the chip represents the on-chip heat bath. The three sets of electrical contact pads are placed at the lower left and right edge of the chip as well as at the bottom edge. The region with most electrical interconnects is well-separated from the octagonal temperature sensors below which the meander-shaped pickup coils are situated.

A novelty of the detectors suited to spectrometry of electron capture (EC) radionuclides is the existence of two on-chip pulser connections that allow applying heat pulses of well-known energy directly to each of the temperature sensors. This feature allows energy-calibrating the detector response without the need for external radioactive sources in future.

The second MMC detector type, named LEX, was newly developed in *MetroMMC* by UHEI for the X-ray emission intensities measurements in the low energy range between 1 and 10 keV at CEA with the highest possible isotope specific absorption probability. The detectors were to meet the following requirements: (i) sensitive area of the detector of about 3 mm^2, (ii) intrinsic absorption efficiency > 99% at 9 keV to yield reliable spectra, (iii) an energy resolution (FWHM) < 10 eV.

A pixelated absorber design combined with a small-scale detector array consisting of four individual MMC detector elements was chosen. This approach was consistent with available SQUID channels as well as the associated DAQ systems at CEA and PTB. Given the pixelated absorber, the 'dead' area between the different absorber elements was minimised to, correspondingly, minimise the number of photons not being measured by a detector. In addition, the individual detectors we designed as identical as possible, in particular with respect to intrinsic absorption efficiency as well as the achievable energy resolution. Moreover, because the number of dc bias lines within the cryostats at CEA and PTB were limited, too, the number of lines for detector biasing, i.e. the lines for supplying the field generating current during persistent current preparation, and the heater lines for actuating the persistent current switches were combined so as to minimise the overall lead count. To give flexibility for the printed circuit board design used to electrically connect to the detectors and to handle potential damages after several wiring up procedures, excess wire bond pads were included in the LEX chip layout.

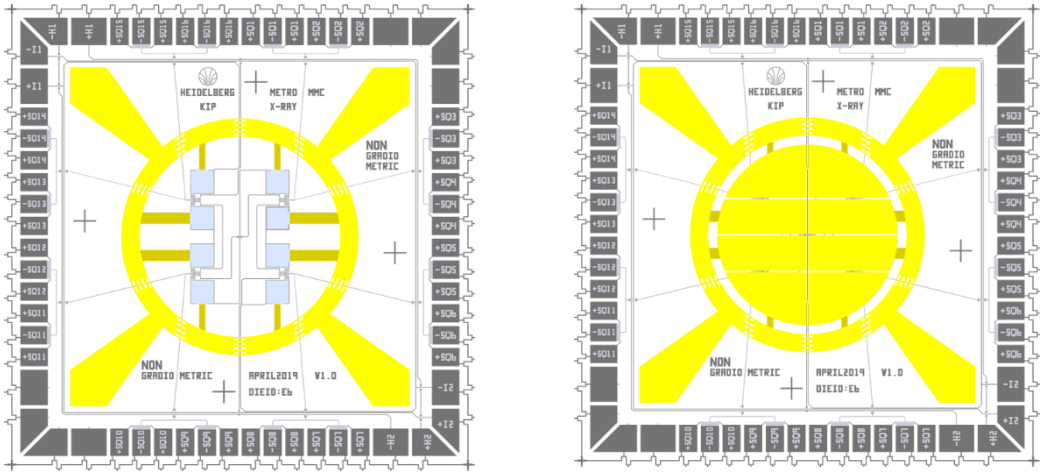

Figure 2: Left, design drawing of the MetroMMC X-ray detector LEX. For better visibility, the absorbers are not shown. Right, design drawing of the MetroMMC X-ray detector with X-ray absorbers.

The microfabrication of both MMC detector types was performed using the same process, i.e. layer sequence, developed at UHEI. The demands on the fabrication of the LEX detectors were, however, significantly more stringent given that (i) several pixels must be combined to the detector array to utilise the total absorber area, (ii) the overhanging, free-standing absorbers only mechanically supported by a very few cylindrical posts, and (iii) a required highly homogenous thickness and size of the different absorber elements.

Table 2: Individual MMC fabrication process steps.

Layer	Material	Process
0	Si-wafer	Si-wafer coated with 240 nm thermally grown SiO_2
1	Nb	Sputter deposition followed by UV-photolithography with positive-tone photoresist and reactive ion etching
2a	Nb_2O_5	Anodic oxidation of first Nb layer using a resist mask created by negative-tone photoresist
2b	SiO2	UV-Photolithography with negative-tone photoresist followed by sputter deposition
2c	SiO2	UV-Photolithography with negative-tone photoresist followed by sputter deposition
3	AuPd	UV-Photolithography with negative-tone photoresist followed by sputter deposition
4	Nb	UV-Photolithography with negative-tone photoresist followed by sputter deposition
5	Au	UV-Photolithography with negative-tone photoresist followed by sputter deposition
6a	Ag:Er + Au	UV-Photolithography with negative-tone photoresist followed by sputter deposition
7	Au	UV-Photolithography with positive-tone photoresist followed by sputter deposition; no lift-off
8	Au	UV-Photolithography with negative-tone photoresist followed by electroplating; no lift-off
9 MMC LEX only	Au	UV-Photolithography with negative-tone photoresist followed by electroplating

High quality source preparation for MMC based decay energy and X-ray emission spectrometry of EC decaying radionuclides is arguably more critical than for MMC based beta decay spectrometry. Within *MetroMMC* the consortium partners CEA and PTB have collaborated strongly and achieved significant technical progress on techniques to prepare both 4π-enclosed source/absorber elements as well as planar source elements for

X-ray emission spectrometry. High-quality sources were produced by electrodeposition of ^{54}Mn and for ^{65}Zn whereas ^{125}I sources were prepared by auto-deposition.

Prior to *MetroMMC*, electrodeposition has already been proven to be very suitable for source preparation for EC measurements with low-temperature detectors, introducing only very small distortions in the measured spectrum, e.g., at CEA and LANL, both with ^{55}Fe as the target nuclide. Electro-deposition is, however, usually strongly element specific and requires extensive process development. At PTB, electro-deposition recipes have been developed for ^{54}Mn and ^{65}Zn for both thin gold foils and standard stainless-steel backings as substrates. Compositions of electrolytes and suitable process parameters for the two substrate materials were found:

Table 3: Electrolyte and process parameters for ^{54}Mn electrodeposition.

Ingredient	**Amount**		**Process parameter**	**Value**
Catholyte			Source diameter	10 mm
HNO_3 with ^{54}Mn	1 ml with ~ 177 kBq ^{54}Mn (1.8.2021)		Distance Anode-Cathode	~8 mm
HNO_3 (pH = 4)	5 ml		Temperature	70 °C
Ultrapure ethanol	1.5 ml		Voltage (set)	30 V
Anolyte			Current (measured)	~1 mA
HNO_3 (pH = 2)	1.5 ml		Duration	~2.5h

Table 4: Electrolyte and process parameters for ^{65}Zn electrodeposition.

Ingredient	**Amount**		**Process parameter**	**Value**
Ultrapure water	8 ml		Source diameter	10 mm
Titriplex III[1] (EDTA)	80 mg		Distance Anode-Cathode	~5 mm
ZnCl	1 mg		Temperature	70 °C
^{65}Zn in ZnCl/HCl based carrier solution	~480 mg with ~32.6 kBq ^{65}Zn (1.8.2021)		Voltage (set)	20 V
0.1 mol/l NaOH	Used to adjust the solution to pH=7		Current (measured)	~300 mA
			Duration	~3 h

At CEA, auto-deposition of ^{125}I onto silver was successfully applied. Iodine cannot be electrodeposited but has a strong chemical affinity with silver. Exposing silver to a solution containing iodine ions will result in the formation of a very thin layer of silver iodide, ideally one single and complete monolayer. In reality this depends on the surface state; as a complete monolayer will most likely only form on a freshly prepared, highly polished silver surface in presence of a sufficiently concentrated iodine solution. Using the solution available in *MetroMMC* (massic activity 3.2 MBq/g; carrier concentration 50 µg/g NaI) an activity of 10 Bq, as typically needed for source/absorbers for MMC-based spectrometry could be deposited onto silver foil of a fraction of a mm^2 in size. Since it was not known in how far a complete silver iodide monolayer would form, four sources with different activity levels (1.4 … 0.14 kBq per 1 mm^2 silver foil area) were prepared. After drying of the solution, the silver foils were rinsed with water to remove crystallisations that might lead to spectrum distortion. The sources should essentially consist of a very thin AgI layer and have higher spectroscopic quality than standard drop deposited sources consisting of a dried compound crystallised in arbitrary crystallite sizes. Subsequent autoradiography revealed the activity distribution within each source. After determination of the approximate activity density from the autoradiography, small parts of the source foil were cut out. To further enhance the spectroscopic quality of the source, the cut-off piece of the source foil was repeatedly folded, laminated and diffusion welded, thus spreading and incorporating the active material into the silver foil volume. This technique, referred to as “kneading”, can considerably reduce the spectrum distortion due to the presence of salt crystallisations in 4π measurements. It can also be used to improve the quality of standard drop deposited sources. It has been shown that with an increasing number of kneading cycles the radioactive deposit is broken to ever smaller particles, reaching a nanometric scale after at least ten cycles.

Measurements of absolute X-ray emission intensities using the novel MetroMMC LEX detector, required the development of data acquisition and analysis to co-add spectra obtained from different detector elements. It is known that nominally identical MMCs can show different sensitivities, read-out noise levels and non-linearities. Consequently, co-adding their individual spectra to obtain a total spectrum to be analysed cannot be performed by a simple addition, as this would result in deformed, non-Gaussian peak shapes and degraded energy

resolution. At CEA, procedures have been developed within *MetroMMC* to correct individual detector non-linearities before the spectra co-adding. In this approach, the differences between measured energies, based on the calibration using only one reference energy, and the calibration energies, obtained from databases, are fitted using a 2nd order polynomial function. After this function was obtained, it allowed correcting each pulse energy for the individual detector elements. When the energy resolutions between pixels were too different (more than 20%), it was found to be more reliable to equalise the energy resolution of the pixels to the poorest one. With regard to the individual detectors' energy resolution, its dependence on energy was fitted using a polynomial function for each detector. Different energy resolutions were degraded by adding to each pulse energy a random energy contribution having a standard deviation determined from the polynomial functions of each pixel.

Additionally, a microwave coupled resonator system has been modelled and designed, based on a 12mm diameter single crystal sapphire resonator, coupled to a 1mm diameter perovskite single crystal at NPL. Both the absorption characteristics for X-rays and the thermal characteristics of the system have been modelled. Construction of the cooler system and thermal characterisation system is completed (figure 3), and we have demonstrated a cooler base temperature of 2.2 K. Further work on another perovskite, CaTiO3 single crystal puck was carried out which showed that below 20K operating temperature the thermal time constant is below 1ms. The heat capacity of the puck was also shown to have a strong T^3 dependence on temperature down to below 10K.

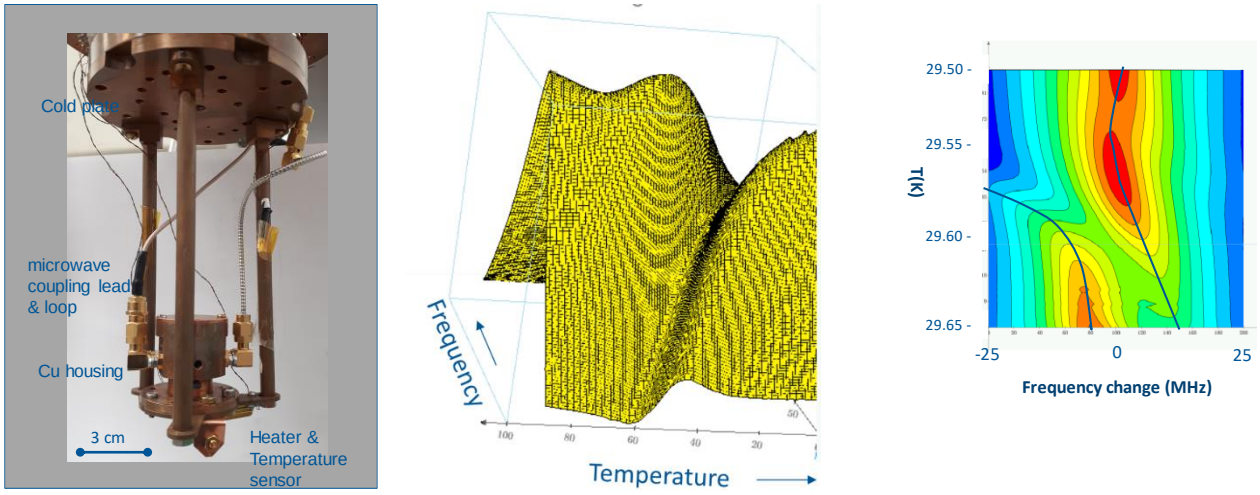

Figure 3: (Left) Photo shows construction of basic MCR system, (middle) Detailed illustration of the frequency vs. temperature dependence of one coupled resonance, (right) a contour plot for f vs.T.

Summary

The key technical achievements of the *MetroMMC* objective *Experimental techniques for spectrometry based on novel cryogenic detectors for radionuclide metrology* lie in the significant advancement of the MMC detector technology and in acquiring the know-how base for the MCR detector approach. With the results on MMC detector design specifically for nuclear decay spectrometry, as well as on source preparation technique and operation of MMC spectrometers from *MetroMMC* partners CEA, PTB and UHEI have established this approach. The above-described results enable the consortium to combine directly MMC spectrometry and activity standardisation in the future as a completely new method for primary activity determination. Furthermore, further development of the MMC spectrometers at CEA and PTB and the MMC data acquisition and analyses provide the foundation to employ this detector type for decay spectrometry that combine highest achievable energy resolution with high statistics (>10^8 decays per spectrum) measurements.

The results achieved with regards to the novel MCR detector provided the groundwork for this approach. All aspects of the novel calorimeter performance were demonstrated, including highly successful demonstration of the required rapid thermal time constant of a coupled resonator, very high df/dT response and promising development of low noise microwave detection system. The comparably high operating temperature makes the MCR approach easier operable and significantly less costly than (very-)low temperature calorimeters. This

way it could provide in future a practical alternative particularly to the spectroscopy of rather short-lived (< few hours) radionuclides.

Determination of fractional EC probabilities of selected radionuclides by means of spectrometry based on novel cryogenic detectors with high energy resolution and very low energy threshold using sources embedded in the detector absorber

Experimental data on fractional electron capture probabilities have been determined within this project for several nuclides using MMCs having the radionuclide source enclosed in the detector absorber thus offering a 4π sr solid angle. The development of the experimental techniques used for this objective have been described in the previous section. In the following, individual source preparation techniques are mentioned and results from the measurements are presented as per radionuclide. Among the six radionuclides chosen for the project, five could be measured; only ^{41}Ca was omitted.

When samples and measurements were carried out with other radionuclides (see below), it became clear that ^{41}Ca measurements would be excessively difficult and only very little ^{41}Ca material was available, deemed too valuable to perform a measurement with only moderate chance of success. In the case of electron capture from the K shell, less than 4 keV are available. A sound measurement of fractional electron-capture probabilities would, however, require measuring at least K and L electron-capture events, the latter providing less than 400 eV only. The corresponding peaks should be clearly distinguishable from each other and clearly distinguishable from the threshold. Moreover, it is to be noted that the half-life $T_{1/2}$ of ^{41}Ca (~10^5 y) is rather long. The activity can be expressed as $A = \ln 2 \times N/T_{1/2}$ with N being the number of atoms. Consequently, samples with an activity of a few Bq could only be prepared with quite substantial amounts of the material (salt) which would have further non-radioactive atoms. Such significant amounts of the material would cause complications in sample preparation and the measurements as disturbing self-absorption and crystal excitation processes would occur. In view of this and the fact that the other measurements have already proved extremely difficult, the consortium has agreed to omit the ^{41}Ca MMC measurements.

^{54}Mn

The source for the 4π measurement of ^{54}Mn was prepared using a PolyPico “PicoSpotter” microdrop dispensing device. It was known from an earlier measurement of ^{65}Zn with a source prepared in the same way, that even the small crystallisations forming from the very small droplets deposited by such a device can significantly distort the spectrum. Therefore, the ^{54}Mn solution was deposited into a gold nanofoam sample fabricated in advance on the surface of a gold half-absorber. The pores of the nanofoam, in the 10s of nm to ~ 100 nm scale, further restrict the size of the crystallisations. Figure 4 shows the spectrum measured with this source.

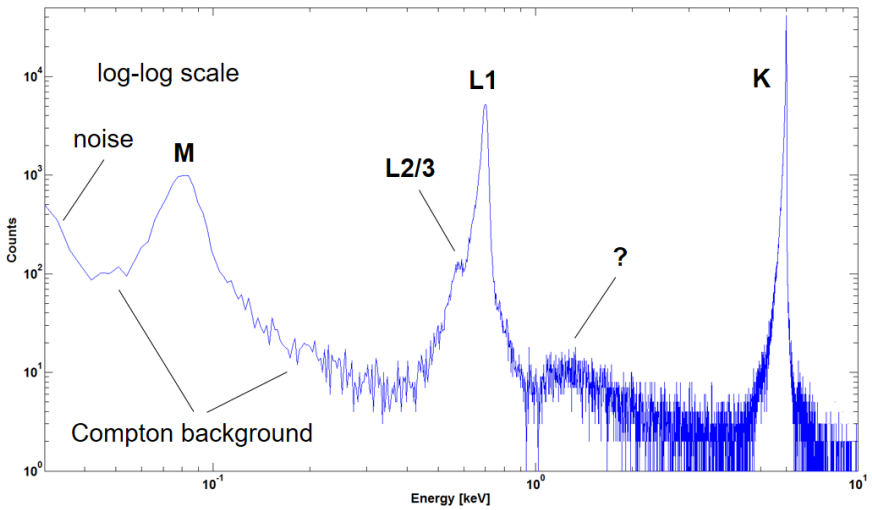

Figure 4: Spectrum of ^{54}Mn measured with an MMC in 4π geometry, i. e. with the ^{54}Mn source embedded in the MMC gold absorber. The Compton background is due to the 835 keV γ emission of the daughter nucleus ^{54}Cr.

The spectrum exhibits a small population at higher energy (around 1.2 keV) than the L capture main line (L1, 700 eV), but much lower than the K capture line (6.0 keV). This spectral feature is broader than the K, L or M lines. It is likely that it is a satellite structure of the L capture peak, as a theoretical spectrum of the electron capture of ^{65}Zn suggests. In the absence of a full theoretical spectrum of ^{54}Mn, we indicate here two sets of fractional capture probabilities, for both hypotheses:

I) The spectral feature around 1.2 keV is a satellite structure of the L capture population and is accounted for as such;

II) It is a spectral artefact of unknown origin and the L capture peak area does not take account of it.

The direct outcome of the measurement are the ratios of the fractional capture probabilities P_L/P_K and P_M/P_K. Since the energy of the N captures lies below the energy threshold of the detector, absolute fractional capture probabilities can be inferred only using theoretical values for P_N. We have used the value calculated with the code BetaShape developed within the EMPIR projects *MetroBeta* and *MetroMMC*. The values for the fractional capture probabilities and for their respective ratios for both scenarios (I) and (II) are compiled in table 5.

Table 5: Fractional capture probabilities P_K, P_L and P_M for ^{54}Mn and their respective ratios, established under the assumptions (I) and (II) concerning the nature of the population around 1.2 keV.

Including the 1,2 keV population in P_L		Not including the 1,2 keV population in P_L		BetaShape	
Fractional capture probability ratios					
P_L/P_K	0,1145 (39)	P_L/P_K	0,1122 (35)	P_L/P_K	0.11219 (31)
P_M/P_K	0,01686 (28)	P_M/P_K	0,01686 (28)	P_M/P_K	0.01746 (11)
Fractional capture probabilities					
Using P_N = 0,001177 from BetaShape		Using P_N = 0,001177 from BetaShape			
P_K	0,88285 (340)	P_K	0,88463 (315)	P_K	0.88419 (34)
P_L	0,10109 (308)	P_L	0,09929 (281)	P_L	0.09920 (23)
P_M	0,01488 (21)	P_M	0,01491 (21)	P_M	0.01544 (9)

^{59}Ni

The preparation of the ^{59}Ni measurement at PTB was very similar to the one for ^{54}Mn at CEA. The absorber was formed from two 25 µm thick gold foils and the source was drop deposited with a microdrop dispenser model MD-P-821 from Microdrop Technologies into a gold nano foam sample. Because of the larger absorber, an S-sized MMC was the matching detector used for the measurement.

Even though both sources of ^{54}Mn and ^{59}Ni were prepared in gold nano foam, the ^{59}Ni measurement exhibits much stronger scattering and distortions to the spectrum shape, attributed to the dielectric source material. But because of the much longer half-life of $T_{1/2}(^{59}\text{Ni}) = 76(5)\times10^3$ as compared to $T_{1/2}(^{54}\text{Mn}) = 312.19(3)$ d, much more material needs to be deposited to reach the desired activity of about A = 10 Bq, which will enhance the scattering effects independent of the host material.

The spectrum shown in figure 5 is quite simple because of the pure electron capture decay of ^{59}Ni without any additional decay channels. The main peak of the K-capture is at 7.7 keV with a secondary edge at 7.1 keV caused by scattering effects. The L-capture is visible at energies around 0.9 keV and can be sub-divided into L1-capture around 0.90 keV and L2-capture around 0.76 keV. Below 0.6 keV we will not try to interpret the spectrum further, since this part is influenced by several factors, including trigger efficiency, background, scattering and “real” events, which are too difficult to disentangle. The continuum between K- and L-captures is mostly treated as background, even though a treatment similar to the 1.2 keV population in the case of ^{54}Mn would also be reasonable.

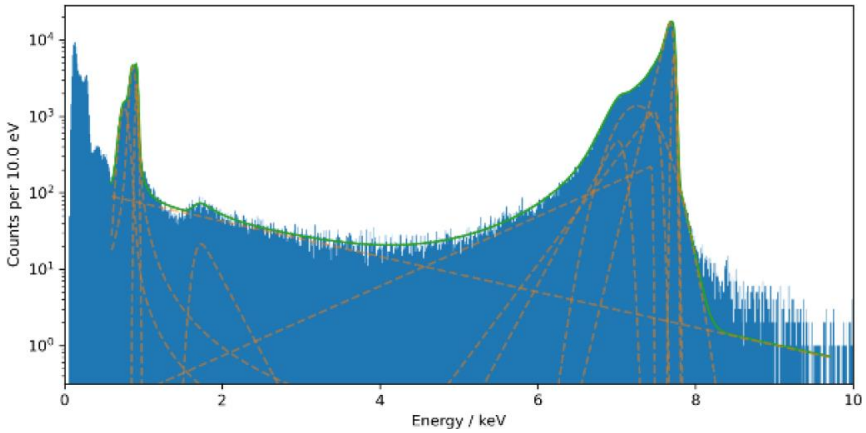

Figure 5: The ^{59}Ni spectrum measured with a drop deposited source in a gold absorber on an S-MMC.

The lines and the background are empirically fitted with a mix of Voigt line shapes and extended Gaussian line shapes with both high and low energy tailing to describe the observed shape including the background. The combined area of the fit functions was used to determine the relative capture probabilities as shown in table 6. Some values show significant discrepancies to the values of BetaShape, which is not surprising because of the difficulty to describe the decay theoretically, because of its 2nd forbidden non-unique nature.

Table 6: Experimental electron capture probabilities as determined from empirical fits to the ^{59}Ni measurement with a drop-deposited source in gold nano-foam. The experimental values are compared to the theoretical values from BetaShape.

Experimental		BetaShape	
Fractional capture probability ratios			
P_L/P_K	1.575E-01	P_L/P_K	1.159E-01
P_{L1}/P_K	1.182E-01	P_{L1}/P_K	1.147E-01
$P_{L2\text{-}3}/P_K$	3.925E-02	$P_{L2\text{-}3}/P_K$	1.180E-03
Fractional capture probabilities			
Using P_M =	1.613E-02	from BetaShape	
Using P_N =	9.760E-04	from BetaShape	
P_K	8.492E-01	P_K	8.808E-01
P_L	1.337E-01	P_L	1.021E-01
P_{L1}	1.004E-01	P_{L1}	1.613E-02
$P_{L2\text{-}3}$	3.217E-04	$P_{L2\text{-}3}$	1.039E-03

^{65}Zn

By the time of the final ^{65}Zn measurement, the electrodeposition of this nuclide had been developed for the X-ray measurements and was successfully used in the preparation of the sample attached to an S sized MMC. The spectrum very cleanly shows the K, L1 and L2 lines. Unfortunately, the detector did not perform as well as expected and the resulting higher energy threshold caused a very low trigger efficiency for the M1 line at around 120 eV. The lines were fitted to empirically describe the observed shape including the background and the combined area of the fit functions was used to determine the relative capture probabilities as shown in table 7. The values from BetaShape are also given as a comparison. To calculate the absolute fractional capture probabilities, values for the probabilities not accessible to the measurements are necessary and values from the program BetaShape were used.

Table 7: Experimental electron capture probabilities as determined from empirical fits to the ^{65}Zn measurement with the electrodeposited source. The experimental values are compared to the theoretical values from BetaShape.

Experimental		BetaShape	
Fractional capture probability ratios			
P_L/P_K	1,156E-01	P_L/P_K	1,191E-01
P_{L1}/P_K	1,120E-01	P_{L1}/P_K	1,183E-01
P_{L2}/P_K	3,621E-03	P_{L2}/P_K	8,298E-04
Fractional capture probabilities			
Using PM =	1,660E-02	from BetaShape	
Using PN =	9,170E-04	from BetaShape	
P_K	8,806E-01	P_K	8,779E-01
P_L	1,018E-01	P_L	1,045E-01
P_{L1}	9,864E-02	P_{L1}	1,038E-01
P_{L2}	3,188E-03	P_{L2}	7,282E-04

^{109}Cd

A ^{109}Cd source of about 10 Bq was drop-deposited onto gold; the 2 x 100 µm gold absorber containing the source best matched an M-sized MMC.

Figure 6 shows the measured spectrum up to 200 keV with low energy tails and other shape distortions apparent in the spectrum due to scattering inside the source material as described previously. Especially the electron capture lines seem to exhibit a double-line shape (more clearly seen in the inset) that could not conclusively be explained up to this point. Because of the higher energies, especially the 88 keV γ transition, the spectrum is much busier compared to the previously described spectra of other nuclides. Since the absorber was not optimised to capture high-energy photons, X-ray escape lines are visible in the spectrum. In addition, the rise time of the detector was rather slow (~1 ms); in combination with the rather high count-rate (>10 s^{-1}) this leads to relatively many pile-up events that need to be considered when determining the capture probabilities.

All the lines were identified, empirically fitted and the resulting areas were attributed to one line (or several in case of pile-up) or designated as background and subsequently used to calculate the electron capture probabilities of the lines with the results shown in table 8. As described previously, to calculate the absolute fractional capture probabilities, values for the probabilities not accessible to the measurements are necessary and values from the program BetaShape were used.

A second way to determine absolute fractional capture probabilities ("with gamma") uses the fact that ^{109}Cd always decays to a long-lived ($T_{1/2}$ = 39.7 s) excited state of the daughter atom ^{109}Ag. Therefore, for basically all decays we will measure the electron capture independent of the accompanying γ transition. In addition, the γ transition is highly converted and mostly emits conversion electrons, only emitting γ photons in 3.66% of decays, reducing the correction needed for reduced high-energy photon absorption in this measurement. The resulting fractional capture probability p_i (i = K, L, M…) can be calculated as:

$$p_i = \frac{n_i}{n_\gamma}$$

with n_i and n_γ being the number of events observed for the electron capture line or the γ transition, respectively.

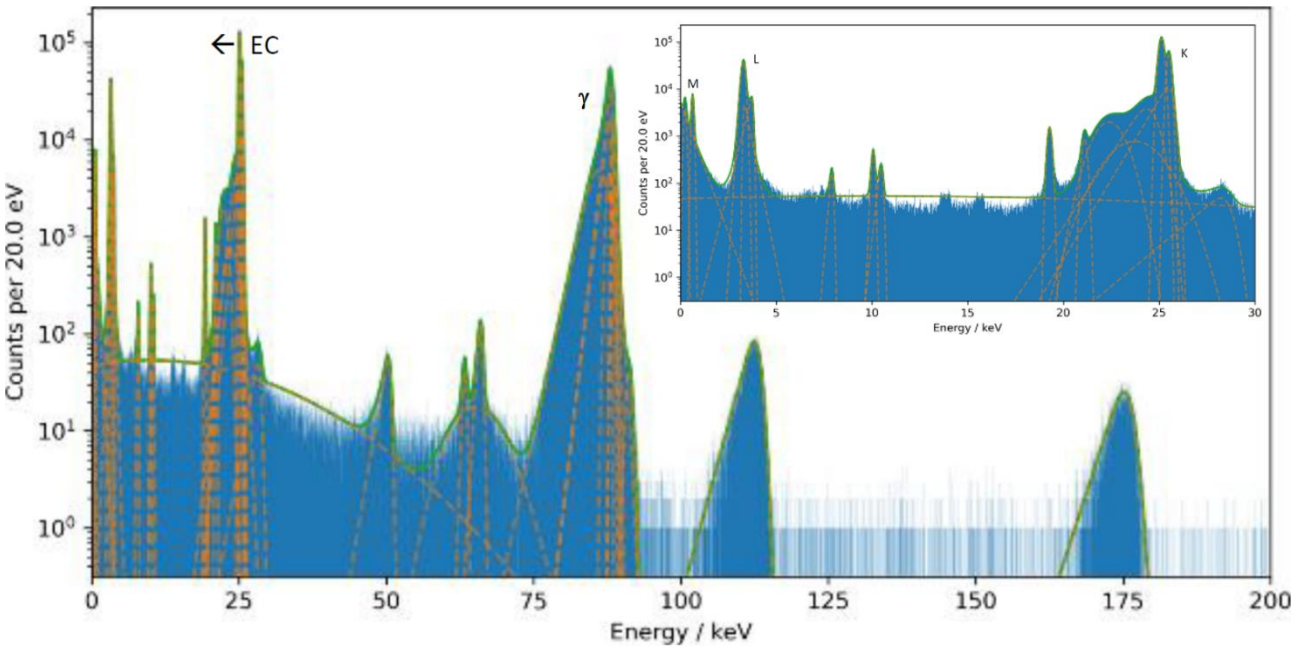

Figure 6: The measured ^{109}Cd spectrum with the gamma line at 88 keV indicated in the figure and the main electron capture part below 26 keV. All other lines are either X-ray escape or pile-up lines. The inset shows the electron capture part of the spectrum with the K, L and M double lines indicated.

As can be seen in table 8, the two methods deliver rather different values for the fractional capture probabilities. Since the results from the first method are closer to the theoretical ones, these seem to be more trustworthy. This discrepancy also points out that there are still some general inconsistencies in this analysis with the root cause currently unknown.

Table 8: Experimental fractional capture probabilities and their ratios as determined from empirical fits to the ^{109}Cd measurement. The capture probabilities are determined in two different ways as described in the text.

Experimental				BetaShape	
Fractional capture probability ratios					
P_L/P_K	1,871E-01			P_L/P_K	1,783E-01
P_M/P_K	1,520E-02			P_M/P_K	3,954E-02
Fractional capture probabilities					
Using P_N =	7,030E-03	from BetaShape			
Using P_O =	4,360E-04	from BetaShape			
with theo. values		with gamma		BetaShape	
P_K	8,255E-01	P_K	7,526E-01	P_K	8,150E-01
P_L	1,545E-01	P_L	1,408E-01	P_L	1,453E-01
P_M	1,255E-02	P_M	1,520E-02	P_M	3,222E-02

^{125}I

An ^{125}I source of high spectroscopic quality and suitable for an MMC measurement can be prepared by spontaneous deposition on silver, favoured by the strong chemical affinity between the two elements. As the EC decay is followed by a 35.49 keV gamma transition with 100 % probability, the EC spectrum is shifted in energy by + 35.49 keV, such that K, L, M and N captures are detected well above the energy threshold of the detector. Nevertheless, O captures are not visible in the experimental spectrum as they are too close in energy (~ 120 eV) to be separated from the N captures given the energy resolution of the detector in this measurement (~ 200 eV).

Rather intense escape peaks, due to the escape of Ag K X-rays from the absorber, are present in the spectrum. For the K captures, the sum of the Kα and Kβ escape peak areas correspond to nearly 1 % of the K capture peak area. In contrast, no Au escape peaks are visible. There are also small peaks present due to the escape of 35.49 keV gamma photons; for the K captures, it corresponds to ~ 0.25 % of the capture events. In the calculation of the fractional capture probabilities, the areas of all escape peaks have been summed with the main peaks of the respective electron shell of their origin.

Since the escape of both silver X-rays and gamma photons has been observed, it must be expected that also some Te X-rays (from the daughter atom of the decay) escape from the detector. These escape events are not directly observable by distinct escape peaks in the spectrum, since the resulting energy will correspond to a capture on one of the higher lying electron shells (liberating a lower energy). Therefore, the values for P_L, P_M and P_N must be slightly overestimated, as can be seen in the comparison with the theoretical values from BetaShape. This issue is currently under investigation. The currently best values are summarised in table 9.

Table 9: Experimental electron capture probabilities and their ratios, compared to the theoretical values from BetaShape.

	MMC	BetaShape
	Fractional capture probability ratios	
P_L/P_K	0,2380 (26)	0,19470 (29)
P_M/P_K	0,0570 (16)	0,04467 (22)
P_N/P_K	0,0157 (21)	0,01012 (10)
	Fractional capture probabilities	
P_K	0,7619 (21)	0,79927 (41)
P_L	0,1814 (17)	0,15562 (15)
P_M	0,0434 (12)	0,03571 (16)
P_N	0,0120 (16)	0,00808 (8)

Summary

All measurements for this objective were performed using Metallic Magnetic Calorimeters with the radionuclide sources embedded in the radiation absorbers. Since the quality of the sources is of crucial importance for high precision measurements without spectral artefacts, for each nuclide extensive development work had to be invested to achieve highest source quality. In some cases, spectral artefacts like photon escape or unidentified background sources led to discrepancies between the experimental values and theoretical calculations performed within the project.
Nevertheless, experimental values for the fractional capture probabilities could be determined for five radionuclides decaying by electron capture: ^{54}Mn, ^{59}Ni, ^{65}Zn, ^{109}Cd and ^{125}I. Only ^{41}Ca could not be measured due to its very low energy emissions and its long half-life and the objective was fully achieved.

Method to determine absolute X-ray emission intensities of selected radionuclides by using a combination of high-resolution spectrometry based on novel cryogenic detectors using external sources and accurate primary activity determination

The aim of this objective was to provide improvements in X-ray emission probabilities for 5 electron capture radionuclides: ^{54}Mn, ^{65}Zn, ^{59}Ni, ^{109}Cd and ^{125}I. Achievement of the objective required work in the following areas: source preparation and activity determination, improvements concerning experimental procedures with Metallic Magnetic Calorimeters (MMCs) as well as the theoretical modelling of these radionuclide' decays. In addition to MMC measurements, the project includes the development of a novel calorimetry concept based on microwave-coupled resonators (MCR).

Source preparation and activity determination

A stainless-steel backing was used for all X-ray sources and ^{54}Mn and ^{65}Zn were directly electrodeposited onto that backing by PTB (see example in figure 7). The other nuclides (^{59}Ni, ^{109}Cd and ^{125}I) were drop-deposited onto a latex pad on the backing, that allowed a more homogeneous distribution of the radioactive solution before drying (see example in figure 8). All sources were covered with a 0.7 µm thin Mylar foil to prevent the Auger electrons from reaching the detector. This work was performed in collaboration between CEA and NPL.

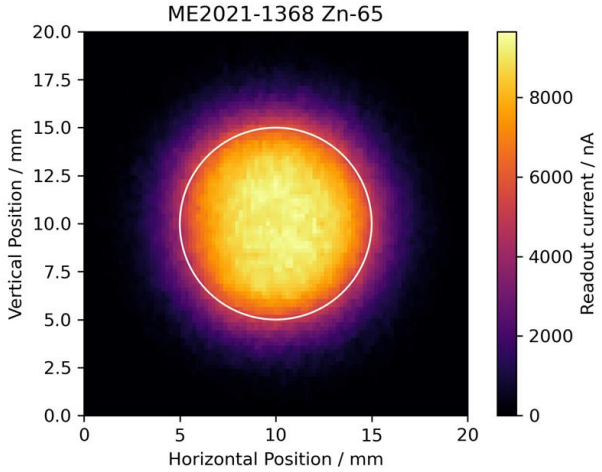

Figure 7: Autoradiographic image of the electrodeposited ^{65}Zn source used for the X-ray emission measurement. *The white circle indicates the nominal source diameter of 10mm.*

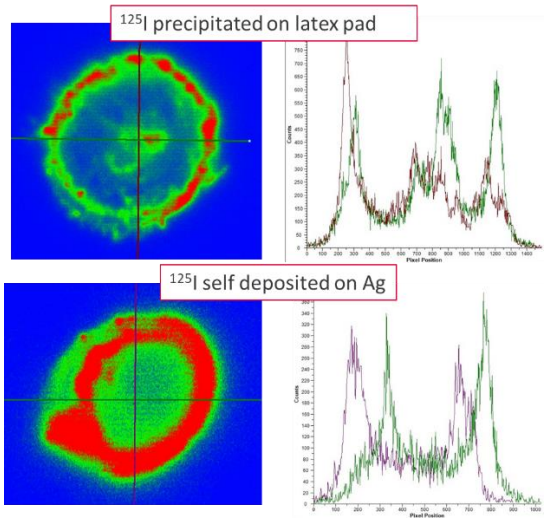

Figure 8: Top left, autoradiographic image of the drop deposited and precipitated ^{125}I source. Top right, activity profiles according to the coloured straight lines on the autoradiographic image. Bottom left, autoradiographic image of the drop and self-deposited ^{125}I source on silver used for the X-ray emission measurement. Bottom right, activity profiles according to the coloured straight lines on the autoradiographic image.

The preparation of electrodeposited sources cannot be controlled gravimetrically. Therefore, the activity cannot be traced back to the master solution and needs to be determined for each source individually. PTB operates three ionisation chambers that are very well characterised and used for secondary activity standardisation. There are established calibration factors for a number of nuclides, including ^{65}Zn and ^{54}Mn. The calibration for ^{65}Zn is based on 4πβ-γ-coincidence counting using a pressurised proportional counter as beta detector, while the calibration for ^{54}Mn was done with 4πβ-γ-coincidence counting using a proportional counter at ambient pressure. The uncertainties of the calibration factors are about 0.75% and 0.45%, respectively.

The radioactive solution of ^{59}Ni provided by NPL was standardised at CEA by liquid scintillation (LS) using the Triple to Double Coincidence Ratio (TDCR) method. Two batches of LS samples were prepared with plastic vials filled with 15 mL of liquid scintillator (Ultima Gold and Hionic Fluor) mixed with aliquots of the master solution. Potential ^{63}Ni impurity was checked by LS spectrometry using a commercial system. TDCR counting was carried out with a detection set-up equipped with BURLE 8850 photomultipliers. The maximum experimental TDCR values were equal to 0.4 for UG samples and 0.274 for HF samples. For activity determination, the detection efficiency was calculated using the KLM model for electron-capture emitters. Coherent results were obtained from counting given by both UG and HF samples. Calculations were also implemented using DDEP and BetaShape nuclear data. The activity concentration at the reference date was

given with an uncertainty equal to 1% due to measurement statistics and nuclear data variation (PK and PL values).

The mass activity of the ^{109}Cd solution was standardised by ionisation chamber with an uncertainty of 0.9%. The presence of impurities was checked by gamma ray spectrometry with an HPGe spectrometer. The ionisation chamber was itself calibrated by radioactive solutions standardised by LSC using the TDCR method.

MMC Measurements

From the experimental point of view, very high energy-resolution is necessary to resolve the complex X-ray spectra and to avoid *a priori* knowledge and assumptions, which have been shown to result in significant systematic errors, especially in the determination of photon emission intensities. To this end, high energy resolution Metallic Magnetic Calorimeters (MMCs) were developed and utilised in this project. Moreover, the employed MMCs have a nearly constant intrinsic detection efficiency that minimises the uncertainties related to the efficiency correction. The 5 radionuclides emit X-rays in two distinct energy ranges: ^{54}Mn, ^{59}Ni and ^{65}Zn emit X-rays between 0.5 keV and 9 keV; and ^{109}Cd and ^{125}I emit mainly K-rays between 20 keV and 35 keV. Therefore, two MMCs with complementary detection efficiency were used by CEA:

- The MMC SMX3, dedicated to photon spectrometry below 50 keV. It was developed prior to this project, with a constant detection efficiency between 5 keV and 25 keV close to 100% and with an energy resolution of about 30 eV.
- The MMC LEX, dedicated to photon spectrometry below 10 keV. It has been developed during this project, and has shown a nearly constant detection efficiency, close to 100% between 1 keV and 10 keV, with an energy resolution of below 10 eV.

A key aspect of high-resolution spectrometry is the capability to manufacture high quality radioactive sources. X-ray emission intensities have been measured for ^{109}Cd, which decays to ^{109}Ag by electron capture to a gamma excited state of 80 keV, the latter is strongly converted. Therefore, the K vacancies are produced by the electron capture followed by the internal conversion leading to 102.2(9) K X-rays and 10.37(27) L X-rays per 100 decays. The source of ^{109}Cd was drop deposited on a stainless-steel disk previously prepared with a 10 mm diameter latex pad. The source was measured during 7 days at 14 mK using the SMX3 MMC. The pulse energies were determined after optimal filtering. Energy spectrum of the K X-ray range of Ag (daughter atom of ^{109}Cd) and its processing is showing in fig 9. Energy spectrum of the L X-ray range and its spectrum processing for ^{109}Cd is showing in Fig. 10.

Once the peak areas are derived from the spectrum processing, they have to be corrected for the detection efficiency. The efficiency of the MMC SMX3 was calibrated using a standard source of ^{241}Am and using Monte Carlo simulations. The efficiency correction concerns mainly the gamma-ray line at 88 keV, due to photon transmission through the absorber, and the L X-ray lines, due to the absorption in the Be window and in the Mylar covering the source.

Once the peak areas are corrected for the efficiency, the photon intensity ratios between two peaks (or groups of peaks) can be calculated. Comparing with the available published values shows a good agreement between the calculated values and the present work for the X-ray ratios. Intensity ratios between X-ray and gamma lines or groups, obtained experimentally from the measurement of ^{109}Cd, were compared with those calculated or evaluated.

The source of ^{125}I was self-deposited on a silver foil to form silver Iodide. This source is expected to be very thin, because the iodine will attach only to the first atoms of silver on the surface. The source had an activity of 2099(31) Bq and was measured during 13 days with the SMX3 MMC. The energy resolution in the spectrum is 37 eV in the K X-ray energy range with a counting statistics of 1.8×10^6 counts.

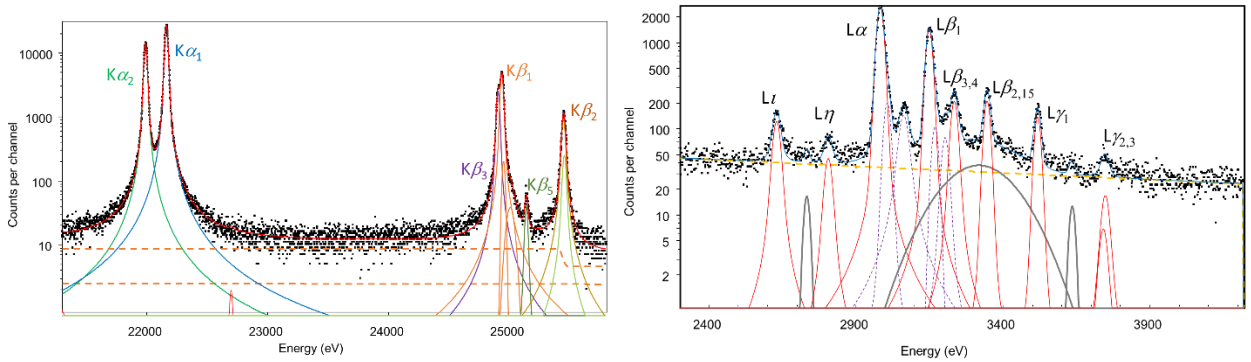

Figure 9 (left): Energy spectrum of the K X-ray range of Ag (daughter atom of ^{109}Cd) and its processing. The red solid line represents the total resulting fit, the dashed lines are the background modelling and the other lines are the K X-ray peaks fitted with Voigt functions.

Figure 10 (right): Energy spectrum of the L X-ray range and its spectrum processing. The blue solid line represents the total resulting fit, the orange dashed line is the background, the red solid lines are the diagram L X-ray lines, the purple dashed lines are satellite lines. The grey solid lines are unidentified contributions.

For ^{125}I energy spectrum of the K X-ray range and its processing were carried out using Colegram. Energy spectrum of the L X-ray range and its spectrum processing were also done by using Colegram for ^{125}I. The detection efficiency for ^{125}I has been corrected in a similar way as for ^{109}Cd. A very good agreement is observed with the evaluated data from the DDEP for the K X-ray ratios.

^{65}Zn decays to ^{65}Cu by EC with a branching ratio of 50.23% to an excited level at 1115 keV and 48.35% to the ground state, with the remaining 1,421% going into a β^+-decay. The source of ^{65}Zn was electroplated with an activity of 9.3 kBq at the measurement date 17/09/2021. The recommended value for the K X-ray emission probability is 39.5(4) photons per 100 decays. The source was measured with the MMC LEX produced during this project. It was measured during 4 days at a temperature of about 16.2 mK, higher than the usual base temperature of the cryostat due to large power dissipation of one two-stage SQUID. The K X-ray energy spectrum from the ^{65}Zn decay shows a resolution of 6.6 eV and a counting statistics of 190000 counts. The L X-rays of ^{65}Zn are measured around 950 eV and shows that the statistics is low but sufficient to process the main peaks with Voigt functions. Intensity ratios between X-rays or groups, obtained experimentally from the measurement of ^{65}Zn have been compared with those calculated or evaluated.

^{59}Ni decays to ^{59}Co by EC with a branching ratio of nearly 100% to the ground state. The recommended value for the K X-ray and L X-ray emission probabilities are 34.4(4) and 0.98(7) photons per 100 decays respectively. The source of ^{59}Ni was prepared by drop deposition on a stainless-steel disk previously prepared with a 10 mm diameter latex pad. The source activity is about 5.1 kBq. It was measured with the MMC LEX produced during this project at about 16.2 mK for 5 days. For the same reasons as ^{65}Zn, the K X-rays lines in the present spectrum were fitted using at least two Voigt functions per transition. With a resolution of 6.0 eV it is not very far from the baseline resolution of 5.6 eV with a statistics of 230000 counts. The L X-ray peaks are almost invisible in the spectrum probably due to strong self-absorption in the source. Indeed, the source was dried after drop deposition and the source autoradiography shows that the activity is concentrated on the outer part of the source diameter leading to a thick deposit.

^{54}Mn decays to ^{54}Cr by EC with a branching ratio of nearly 100% to the excited state of 835 keV. The recommended value for the K X-ray and L X-ray emission probabilities are 25.7(5) and 0.65(13) photons per 100 decays respectively. The source was electroplated on a stainless-steel disk with an activity of 24.2 kBq. The temperature of the detector was about 14.5 mK. The statistics is 235000 counts in the K X-ray range. For the same reasons as ^{65}Zn, the K X-rays lines in the present spectrum were fitted using at least two Voigt functions per transition. The resolution of about 5 eV hardly separates the Kα lines making the spectrum processing difficult. In addition, the Kβ lines have a strange shape, with a left tail and a left bump. The L X-ray peaks near 500 eV are very weak in the spectrum but quantifiable. Table 10 compares the measured ratios to those from calculations or evaluations.

In addition, we compared the experimental ratios to the evaluated and calculated data available in the literature, and to the results of the sophisticated calculations performed during this project (see D4 report).

Table 10: Intensity ratios between X-rays or groups, obtained experimentally from the measurement of ^{54}Mn, compared with those calculated or evaluated.

Ratio	Scofield Z = 24 [7,8]	DDEP [13]	This work
Kβ/Kα	**0.13370**	0.1345 (36)	0.1327 (23)
$K\alpha_2/K\alpha_1$	**0.50910**	0.509 (13)	0.4319 (35)
$K\beta'_1/K\alpha_1$	**0.20180**	0.203 (6)	0.1900 (33)
L/K		0.025 (5)	0.0114 (14)

MCR Realisation

Additional to MMC measurements, this objective includes the development of a novel calorimetry concept, based on microwave-coupled resonators (MCR). This concept, which couples together two different microwave dielectric resonators, presents attractive features that in future may make it a promising alternative to MMCs. Non-contacting interrogation is done by the microwave field itself, and no cables are required to contact the sensor. Also, since the absorber is an insulator, it has minimal heat capacity, only due to phonons, with no conduction electron contribution (unlike metal or semiconductor calorimeters). For T < 5 K an insulating sensor can have a much smaller heat capacity than a metal one of similar mass at the same temperature. Thus, a dielectric sensor may provide higher energy resolution than a metallic one or alternatively it could achieve the same resolution but be operated at a higher temperature, reducing cryogenic complexity. Furthermore, the physical volume of the perovskite resonator (~1 mm^3) is several orders greater than that of thin film sensors, and more compatible with the absorption lengths associated with 1 keV to 10^3 keV X-rays (the proposed energy range of this detector), which may be as large as 1 mm. The prototype work reported here predicts an energy resolution of < 10 eV and a time constant of 1 ms, achievable at temperatures ~4 K, thus opening many potential radiation-detection applications.

Within this objective, relating to the MCR developments, NPL has developed new hardware, a fast data acquisition system, and microwave interrogation based on a heterodyne detection approach (figures 11 and 12). NPL has also developed a pulse acquisition system based on taking the output of our detection system and converting the analogue signal to a stream of pulses by digitising and then digitally filtering the output stream. A very weak (200 Bq) ^{241}Am source was included within the copper housing of the coupled resonator system, spaced 4 mm away from the absorber. Calculation of the solid angle subtended by the absorber by the ^{241}Am source predict a detection rate of approximately 0.25 counts/sec of the emitted 5 MeV alphas. The MCR system was cooled to a temperature of 28.5 K where the temperature dependence *df/dT* was maximised for this setup. A detection system was set up to detect individual pulses with a resolution of 200 µs. The MCR system was used for characterisation measurements, both with an alpha-emitter (^{241}Am) and microwave calibration pulses injected into the microwave resonator, which could be clearly identified and showed a duration of about 1 ms, consistent with expectations. This has led to the first demonstration of particle detection using an MCR and a paper has been published.

A key part of the development of the technique relies on material testing, we have detailed a useful comparison between the key dielectric single crystal materials, $SrTiO_3$ and $CaTiO_3$, both perovskite compounds, which show paraelectric behaviour down to low temperatures.

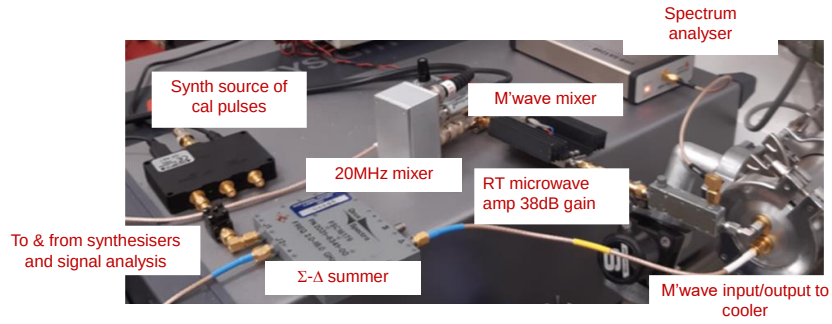

Figure 11: Photo of improved microwave heterodyne readout system at room temperature.

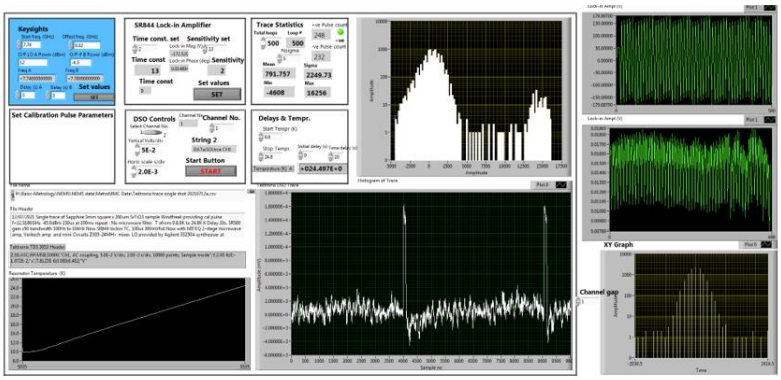

Figure 12: Labview Software front panel for controlling and collection the data.

Conclusion

For source preparation, a stainless-steel backing was used for all X-ray sources and ^{54}Mn and ^{65}Zn were directly electrodeposited on that backing. The other nuclides (^{59}Ni, ^{109}Cd and ^{125}I) were drop deposited onto a latex pad on the backing, that allowed a more homogeneous distribution of the radioactive solution before drying. All sources were covered with a 0.7 µm thin Mylar foil to stop the Auger electrons from reaching the detector. Measurement methods employed for activity determination used a pressurised proportional counter as beta detector, standardised by ionisation chamber with an uncertainty of 0.9%. The presence of impurities was checked by gamma ray spectrometry with an HPGe spectrometer.

Two different MMC systems were used for the X-ray measurements, the MMC SMX3, that had already been developed, characterised and used for several measurements before the project. This system is optimised for photon energies up to 26 keV, but its photon absorption characteristics were extensively scrutinised using a combination of a well characterised high-energetic (E<100 keV) photon emitter, ^{241}Am, accompanied by Monte Carlo simulations of the whole setup. Due to the higher energy emissions of ^{109}Cd and ^{125}I, these nuclides were well suited to be measured with the MMC SMX3 system.

The newly developed MMC for low energy X-rays below 10 keV, named LEX, was successfully used to measure the remaining nuclides ^{54}Mn, ^{59}Ni, and ^{65}Zn.

The γ-rays of ^{109}Cd and ^{125}I, and the K- and L-X-rays of all nuclides could be identified in the measured spectra and analysed for their relative intensities. Only in ^{59}Ni, the L-X-rays showed a significantly reduced intensity, likely due to self-absorption in the source. The data allowed to analyse the relative X-ray intensities. Absolute intensities could unfortunately not be given, since a sample changer did not become operational in time, which prohibited an in-situ solid angle calibration, which is necessary to give absolute values.

The MCR system was used for characterisation measurements, both with an alpha-emitter (^{241}Am) and microwave calibration pulses injected into the microwave resonator, which could be clearly identified and showed a duration of about 1 ms, consistent with expectations. Unfortunately, due to restricted material properties of the perovskite absorbers, the detector performance and its low-energy threshold were not good enough to significantly contribute to the X-ray measurements.

Overall, we have achieved almost all the activities of the proposed objective. The measurements of high energy resolution X-ray spectra of the 5 planned radionuclides (^{109}Cd, ^{125}I, ^{54}Mn, the ^{59}Ni and the ^{65}Zn) were performed using two different MMCs. We have modelled the emission spectra resulting from the atomic relaxation of the daughter atom for all the 5 radionuclides focus of this project. Comparison between experimental and

theoretical X-ray emission intensities has been detailed in the D4 report “Validation report on the effect of improved X-rays measurements”. A novel MCR detector also made good progress and the results obtained in this project have demonstrated for the first time the capability of single particle detection with this novel calorimetric detector and a paper has been published.

Summary

The third objective was to determine X-ray emission intensities of the same radionuclides (^{54}Mn, ^{59}Ni, ^{65}Zn, ^{109}Cd and ^{125}I) using MMCs. In addition to MMC measurements, it includes the development of a novel calorimetry concept based on microwave-coupled resonators (MCR). Apart from the detector development, also the source preparation plays a significant role to measure X-rays accurately to very low energies. Especially at energies below 1 keV, self-absorption in the source material itself can reduce the intensity, while Auger electrons, that are also emitted after the decay, should not reach the detector, since these cannot be distinguished from X-rays with the used detector technologies.

Theoretical models and ab initio calculations of the electron capture process and subsequent atomic relaxation and validation with the high-precision experimental data

Achieving theoretical predictions of electron capture decay and subsequent atomic relaxation process at the percent precision level is highly challenging. This problem was tackled in the present project employing different approaches among the most precise available and comparing the results to measurements.

Electron capture decay

Nuclear physics studies refer to evaluated nuclear data, which can be taken either in the ENSDF (*Evaluated Nuclear Structure Data File*) database or in the DDEP (*Decay Data Evaluation Project*) database, the latter being recommended by the BIPM (*International Bureau of Weights and Measures*) for metrology purposes. In ENSDF evaluations, the properties of beta transitions and electron captures are still calculated with the LogFT code, which is based on an approximate theoretical model limited by the computing power available in the 1970s.

Within the framework of this project, the BetaShape code, originally developed by CEA to improve the theoretical predictions for beta transitions, has been developed further to improve electron capture calculations as well. Its specific model takes precisely into account several important physical phenomena: overlap and exchange effects for each atomic subshell; hole effect due to the vacancy created by the decay process, treated by means of first order perturbation theory; account of total shaking probability (auto-excitation plus auto-ionisation); precise theoretical atomic binding energies from NIST website; and radiative corrections due to quantum electrodynamics. It provides much more detailed information required by different communities, among them radionuclide metrology. Electron capture probabilities as well as capture-to-positron probability ratios were compared to accurate measurements available in the literature and good agreement was found within the precision of the latter. Figure 13 shows the comparison between theory and experiment of capture probability ratios in the allowed decay of ^{55}Fe and the second forbidden unique decay of ^{138}La.

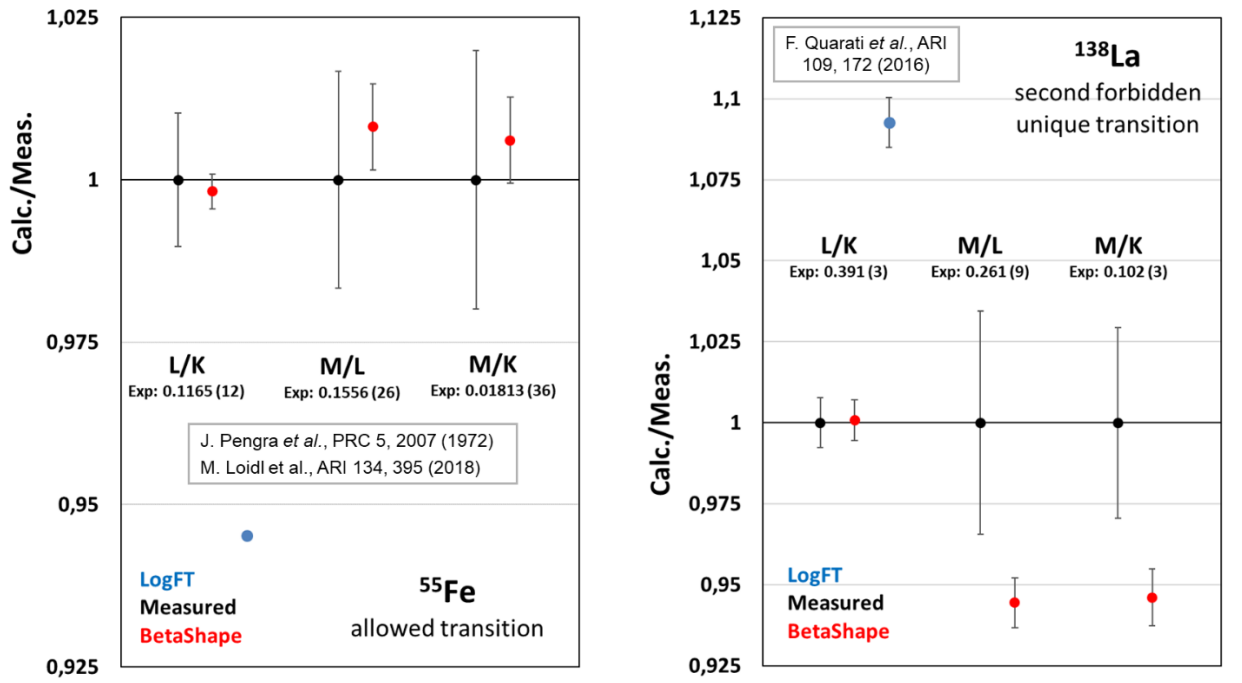

Figure 13: Comparison between theory and experiment of capture probability ratios in the allowed decay of ^{55}Fe and the second forbidden unique decay of ^{138}La. Black points are only measured-to-measured ratios and are presented to illustrate the experimental uncertainty. Blue points are the incomplete results from the historical LogFT code. Red point are from the improved model of the BetaShape code.

The entire DDEP database has been updated with the BetaShape code and the improved data have been made freely available at: http://www.lnhb.fr/nuclear-data/nuclear-data-table/. Executables of the BetaShape code have also been made freely available for various platforms at: http://www.lnhb.fr/rd-activities/spectrum-processing-software/. The DDEP collaboration have adopted this new code for their nuclear data evaluations.

Going a step further requires employing more accurate atomic wave functions and binding energies as an input of this improved model. For this purpose, a realistic atomic model was developed by CNRS within the framework of the relativistic density functional theory, in which several exchange-correlation functionals and self-interaction-corrected models among the most popular in the community were implemented. Correlation effects were studied by comparison with measured binding energies and the best model was selected to generated precise atomic wave functions.

CEA then implemented a specific version of the BetaShape code in order to directly use these wave functions and their energies in the improved electron capture decay model developed in this project. Extensive, very technical discussions were necessary to link the different formalisms used by CNRS and CEA. It is noteworthy that thanks to CNRS code, an exact treatment of the hole effect due to the vacancy created in the capture process was then possible in CEA code. The high-precision measurements from this project were not available at the time of the comparison. It was thus decided to study the influence on capture probabilities of the atomic wave functions from the two different atomic models:

i) the BetaShape model of electron capture that includes an atomic model, developed by CEA; and

ii) the KLI (*Krieger-Lee-Iafrate*) model of atomic structure based on DFT (*Density Functional Theory*), developed by CNRS.

Internal conversion theory was recently tested comparing precise measurements with different predictions. This study is available in the literature and is independent of this project and of the teams involved. Two hypotheses were considered:

i) the “no vacancy” approximation, which assumes a final state corresponding to the daughter atom after full atomic relaxation; and

ii) the “frozen orbital” (FO) approximation, which assumes that the final atomic orbitals in the internal conversion process correspond to those of the parent atom with a vacancy.

It was found that FO approximation gave the most accurate and consistent results over a wide range of atomic numbers, as expected from the time scales of the physical processes.

The situation is comparable for electron capture. The weak interaction transforms the parent nucleus with atomic number *Z* into the daughter nucleus with atomic number (*Z-1*). This interaction is mediated by massive bosons and is therefore of very short range. The time scale of the electron capture decay might thus be seen as instantaneous compared to the atomic time scale, i.e. the vacancy lifetime. The BetaShape model assumes the FO approximation, and the KLI model was considered for both the FO and the "no vacancy" approximations. It is noteworthy that in the latter case, the hole effect is not taken into account.

Table 11: Comparison of calculated and measured capture probabilities for different isotopes.

Isotope	Energy (keV)	Quantity	BetaShape	KLI "no vacancy"	KLI "frozen orbital"	Experimental
^{7}Be	861.89 (7)	P_L/P_K	0.105 (8)	0.1606 (41)	0.0509 (20)	0.070 (7)
^{41}Ca	421.64 (14)	P_L/P_K	0.09800 (40)	0.10415 (16)	0.09078 (16)	–
^{54}Mn	542.2 (10)	P_L/P_K	0.11219 (31)	0.10785 (8)	0.09590 (19)	0.1044 (27)
		P_K	0.88419 (34)	0.88623 (10)	0.90005 (21)	0.901 (6)
^{55}Fe	231.12 (18)	P_L/P_K	0.11629 (31)	0.11236 (8)	0.10073 (20)	0.1165 (9)
		P_M/P_K	0.01824 (12)	0.019390 (32)	0.014824 (45)	0.01786 (29)
		P_M/P_L	0.1568 (11)	0.17257 (31)	0.14716 (49)	0.1556 (26)
^{109}Cd	127.1 (18)	P_K	0.8148 (14)	0.8097 (11)	0.8164 (12)	0.815 (2)
		P_{LMNO}/P_K	0.2274 (12)	0.2350 (11)	0.2250 (12)	0.2279 (21)
^{125}I	150.28 (6)	P_K	0.79927 (41)	0.79798 (7)	0.80376 (23)	0.7971 (14)
^{138}La	312.60 (30)	P_L/P_K	0.3913 (25)	0.4077 (15)	0.4242 (49)	0.391 (3)
		P_M/P_K	0.0965 (9)	0.09908 (41)	0.1002 (11)	0.102 (3)
		P_M/P_L	0.2465 (20)	0.2430 (22)	0.2362 (24)	0.261 (9)

The dominant electron capture transition for each of the radionuclides of interest has been investigated. Calculation of capture probabilities have been performed using the recommended Q-values established in the latest Atomic Mass Evaluation AME2020. The results are given in table 11 together with evaluated experimental values when available. Their analysis highlighted the influence of the different corrections and assumptions.

Atomic relaxation

Two independent, state-of-the-art approaches to treat the atomic many-body problem have been employed in this project. With the first one, UHEI has described as a whole the electron capture process and the subsequent atomic relaxation within Kubo's formalism using Green's functions. During an electron capture decay, a total amount of energy *Q* is released that depends on the initial and final isotopes involved in the process. This energy *Q* is shared between a created neutrino with energy E_ν and electronic excitations of the daughter atom, $E_e = Q - E_\nu$. The electron capture spectrum is defined as the double differential cross section, encoding the partial capture rate in the energy interval E_e to $E_e + \delta E$, i.e. $(Q - E_\nu)$ to $(Q - E_\nu + \delta E)$.

The electron capture process is governed by the weak interaction. At the energy scales of interest, the magnitude of this interaction is small compared to the electromagnetic forces between the electrons themselves or between electrons and protons in the nucleus. The weak interaction can be treated in first order perturbation theory for describing the electron capture spectrum. In the time domain, start is made at time *t=0* by annihilating a core electron from one of the basis functions, changing the nuclear charge from *Z* to *(Z-1)* and simultaneously creating a neutrino. The resulting daughter atom is in an excited state and non-trivially time evolves due to electromagnetic interactions between the electrons and additional photons that can be created. The electron capture spectrum can be calculated from the Fourier transform of the real time evolution.

Within this project, the existing code Quanty (www.quanty.org) originally developed by UHEI for the calculation of core level excitations of atoms, molecules and solids was extended to include explicitly the Auger-Meitner

and fluorescence decays. For the latter, additional photons that are created during the time evolution were explicitly included in the Hilbert space. The photon energy plus the neutrino energy not necessarily equals the total released energy *Q* as additional energy can be stored in electronic excitations of the daughter atom. As such, any photon energy can be produced up to the *Q* energy and the electron capture spectrum becomes non-zero at all energies E_e or E_ν.

In total, UHEI found that the resonances related to the atomic shells are split by multiplets, that additional bound double core hole states arise due to the Auger-Meitner decay into bound states and that the spectral line shape emerges as non-Lorentzian due to the energy dependent decay. The states involved during the fluorescence or Auger decay are neither pure eigenstates of the mother nor of the daughter nuclei. Both decay processes are of similar order whereby for the low energy edges the Auger-Meitner decay dominates, and for the *K* edges the fluorescence decay dominates.

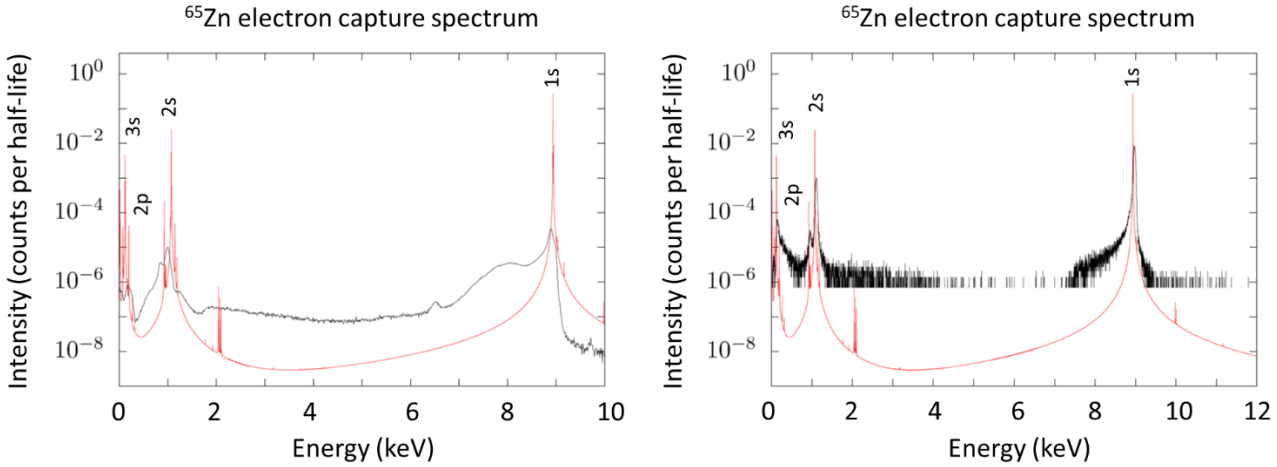

Figure 14: Theoretical electron capture spectrum of ^{65}Zn including Auger decay into bound states compared to two different experimentally measured spectra. One can clearly recognise the different resonances due to the 1s, 2s, 2p and 3s core orbitals. An additional structure at 2 keV is attributed to a double n=2 core hole state with an additional 4p electron.

In figure 14 the theoretical electron capture spectrum is compared with two different experimental spectra for ^{65}Zn. One can clearly see that the theoretical resonances related to the different atomic orbitals are split by additional multiplets. Furthermore, an additional state can be observed at 2 keV related to a double core hole in the *n=2* shell with one additional electron in the *4p* shell. Within an atom this is a bound state, whereas for Zn embedding in a solid the *4p* shell will delocalise, turning the bound state into an edge jump, as one most probably observes in the experiment. Adding the effects of the solid to these types of calculations is needed to obtain the feature at 2 keV with higher accuracy.

The other possible treatment of the many-body problem is the multiconfiguration Dirac-Fock (MCDF) approach, addressed in this project by UNL. The calculations employed the Multiconfiguration Dirac-Fock and General Matrix Elements (MCDFGME) code that implements the MCDF method. In this project, a new computational tool has been developed that allows multithreading the MCDFGME calculations. This tool has made tractable in the timeline of the project the calculation of the millions of X-ray and Auger atomic transitions with unprecedented accuracy. Consecutive to the electron capture process, the emission spectrum and intensities resulting from the atomic relaxation of the daughter atom have been modelled for all the radionuclides of interest (^{109}Cd, ^{125}I, ^{54}Mn, ^{59}Ni and ^{65}Zn). Spectral intensities and natural line widths have been directly compared to the new experimental data obtained in this project.

In an electron capture decay, the creation of an inner-shell vacancy in the atom happens by the capture of an electron by the nucleus. Therefore, a full comparison between experiment data and calculated atomic emission intensities is only possible by using as normalisation of the theoretical intensities with the capture rate for each atomic shell. Yet, if the theoretical spectrum is calculated assuming just the emission, i.e. assuming an identical vacancy creation probability in every shell, the ratio between total emission for two initial configurations matching the experimental spectrum, for instance a vacancy in *K* or *L* shell, gives the capture *K*/*L* probability ratio. Without considering the nuclear decay phenomena probabilities, it is thus still possible to compare X-ray emission intensities between experiment and theory by comparing different X-ray lines coming from the same

initial atomic configuration, e.g. $K\alpha_1/K\alpha_2$ or $K\alpha/K\beta$ ratios. Since the lines are coming from the same initial atomic configuration, neither the capture rate nor the Auger emission affects this ratio, which only depends on the radiative transition to the final state. Figure 15 presents the theoretical energy spectrum determined for ^{109}Cd electron capture decay in the $K\alpha$ energy region.

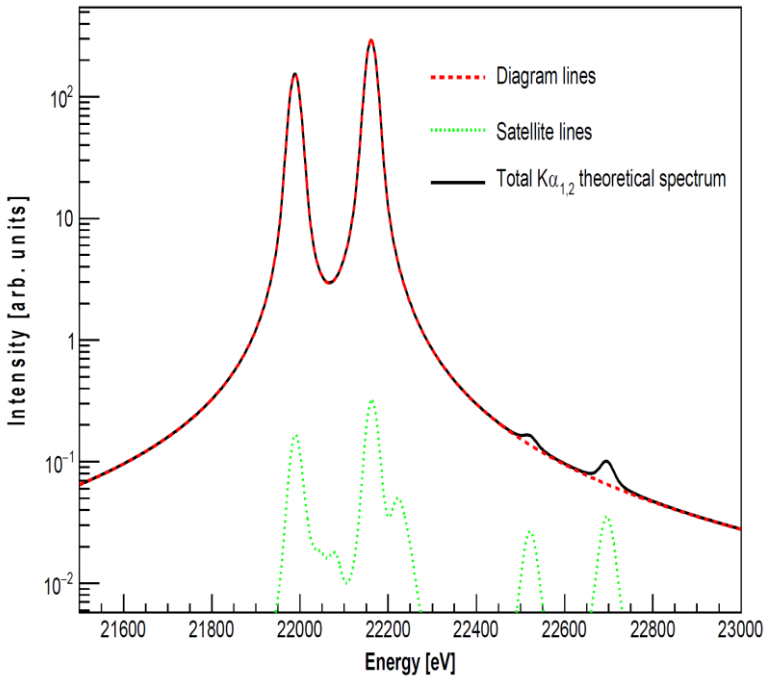

Figure 15: Theoretical spectrum of ^{109}Cd electron capture decay in the Kα energy region. Every possible radiative transition is plotted as a Voigt profile with natural width and relative intensity. The Gaussian width is the experimental energy resolution of the MMC for this energy range (23 eV FWHM). Red dashed curve represents the diagram lines, dotted green curve the satellite lines and the full black curve is the total spectrum.

One of the main implications of the X-ray precision measurements performed in this project is the possibility to benchmark atomic theories. UNL have compared the former to the results of two atomic relaxation theories. The first one was used by J. Scofield 50 years ago, who produced results extensively published in referenced atomic and nuclear data tables. In this case, the X-ray emission rates for the filling of *K*- and *L*-shell vacancies were calculated with the relativistic Hartree-Slater theory for elements with atomic number $5 < Z < 104$. These calculations did account for the extent of nuclear-charge distributions and provided the ratios of the major *K*-shell components, the total *K*- and *L*-shell radiative decay rates, and the rates of emission of individual X-ray lines. The second theory is the much more accurate MCDF method in which UNL have the highest expertise. Table 12 presents a summary of such a comparison in the case of ^{109}Cd electron capture decay. These calculations have not considered the emission of possible satellite lines. While it is not expected that the satellite emissions will have an important effect in the *K* line ratios, one must account for it for a complete comparison. Including these emissions in UNL theoretical calculations has been left to future work. Comparisons to additional high-precision experimental spectra will help to identify and explain features not yet explained such as shoulders and asymmetries present in experimental lines. Moreover, it will be possible to evaluate the contribution of hidden satellite lines on the diagram lines intensity.

Considering the uncertainty of a radiative transition and assuming that radiationless transitions have similar rate uncertainty < 1 %, we can assume that the expected uncertainties on the fluorescence yields for the K, L, and M shells of ~2 %, ~6 % and ~20 %, respectively has been achieved. This uncertainty escalates with the number of transitions, being the reason to have higher uncertainty for the outer shells.

Table 12: Intensity ratios of X-ray and γ lines or groups obtained experimentally for ^{109}Cd electron capture decay compared with those evaluated or calculated from two different theories.

Ratio	Scofield	UNL	DDEP	Experimental (MMC)
$K\beta/K\alpha$	0.2130	–	0.2123 (30)	0.2104 (10)
$K\alpha_2/K\alpha_1$	0.5305	0.5267	0.530 (11)	0.5330 (11)
$K\beta_3/K\beta_1$	0.5138	0.5160	–	0.5079 (27)
$K\beta'_1/K\alpha_1$	0.2775	0.3068	0.277 (5)	0.2714 (7)
$K\beta'_2/K\alpha_1$	0.0484	0.05419	0.0481 (19)	0.05105 (33)
$K\beta_1/K\alpha_1$	0.1694	0.20127	–	0.1791 (6)
$K\beta_2/K\beta_1$	0.2502	0.2687	–	0.2850 (18)
$K\beta_5/K\beta_1$	0.0083	0.008297	–	0.00745 (26)
$K\beta_4/K\beta_1$	0.00093	0.000482	–	0.00047 (8)
K/γ	–	–	27.93 (45)	28.7 (5)
L/K	–	–	0.1015 (27)	0.0924 (24)

Conclusion

The theoretical description of the electron capture decay and of the subsequent atomic relaxation process has been addressed in the present project with the most precise available approaches. An improved model of electron capture has been developed and validated by comparison with precise measurements. This model has been implemented in the BetaShape code, which has been adopted by the DDEP international collaboration as a reference code for nuclear data evaluations. A new DFT code has been developed to determine accurate atomic wave functions. Among the different tested parameterisations, the one giving the best agreement with measured binding energies was selected. This code was coupled with BetaShape, improving further the electron capture model. Comparison with precise data highlighted the influence of the different hypotheses.

Regarding atomic relaxation, two well-established methods for treating the many-body problem had to be improved in order to provide theoretical predictions with a competitive precision compared with the measurements from this project. Electron capture spectra, atomic fundamental parameters such as fluorescence yields and Auger emission probabilities, were calculated for the radionuclides of interest. Influence of electronic correlations up the highest orbitals was studied. An extensive survey of existing data and calculation methods in the literature was performed and non-negligible discrepancies were reported. The most reliable theoretical results were found being from this project.

The percent precision level, and even below, has been reached with these improved theoretical models for the most intense transitions, which are associated with the inner atomic shells and completely fulfils the objective of this project. Much more work is however needed to reach such a precision for the outer shells. Many possible effects usually neglected could be added in the theoretical description. New high-precision experimental data over a large range of atomic numbers are required to give hints for selecting the most important effects in the context of electron capture decay and to benchmark the future theoretical calculations.

5 Impact

The project's results were disseminated in different ways. Stakeholders were identified and invited to join the first Stakeholder workshop in Saclay in October 2019 and a second virtual workshop in December 2021. A workshop was organised in Heidelberg in October 2020 for all those interested in EC spectra calculations using the Quanty program. The wide metrology community was invited to join a training course on nuclear data evaluations, organised by CEA that included the use of several nuclear data relevant software packages. A second training course on liquid scintillation (LS) counting was organised by NPL focussed on the relevance of nuclear data in LS. On ten occasions the project and its results were presented to European and International regulatory bodies. The broader scientific community was the target audience of ten articles in peer-reviewed journals, 18 oral and poster presentations held at national and international conferences and

20 additional presentations held at other external events. News and events as well as links to publications were published on the project website http://empir.npl.co.uk/metrommc/.

Impact on industrial and other user communities

Within the project, uncertainties of nuclear decay data were reduced for a variety of radionuclides. This improved the accuracy of activity standards, which are required for industrial applications. In the case of ^{41}Ca, the newly calculated EC probabilities were used to recalculate its half-life which is relevant for research related to the early history of the solar system and also for radioactive waste management. Since the calculated EC probabilities have lower uncertainties, this reevaluation led also to a half-life with reduced uncertainty. Improved knowledge of the emission probabilities of Auger electrons and X-rays at each energy level is critical for EC nuclides used in nuclear medicine since the estimation of the administered dose greatly depends on these data.

NPL is currently reviewing its procedures for the production of γ-spectroscopy calibration sources. This has already started with ^{109}Cd and will continue for ^{65}Zn and ^{54}Mn. These sources are regularly sold to a variety of customers, and through them the improved nuclear data will increase the confidence in detector calibrations in many fields.

Impact on the metrology and scientific communities

Experimentally determined EC probabilities and X-ray emission intensities have led to improvements of theoretical calculation methods. The measured data and improved calculation methods will be an invaluable contribution to the realisation of the SI unit becquerel in radionuclide metrology. Radionuclide metrologists are now enabled to reduce uncertainties, which is important for several other fields where precise radioactivity measurements matter. This comprises geo- and cosmochronology, nuclear medicine as well as industrial applications, but also research in other fields. The improved calculation techniques of the EC process, and its subsequent atomic relaxation are essential for a sound research of radiation effects in human tissue on the DNA level. Improved calculation methods have already been presented to the “nuclear decay data evaluation community”. Computed fractional EC probabilities of ^{55}Fe obtained from the BetaShape program were recommended by the Key Comparison Working Group (KCWG) of the CCRI(II) and were used by the participants of a recent key comparison on ^{55}Fe. The new EC probabilities had significant influence on the determined activity. As a result, the project already created significant impact within the radionuclide metrology community.

The developments will also contribute to new basic research experiments which require measurements of ionising radiation with high energy resolution. As an example, short baseline neutrino oscillation experiments at nuclear reactors would benefit from accurate EC probability measurements for the indispensable evaluation of background sources.

Beyond the direct impact from the measurements on EC decaying nuclides, the advances in MMC and related readout techniques triggered by this project will be highly beneficial in numerous fields of applied and fundamental research in which MMCs play an increasingly important role. Some of the developments will also be applicable to other types of cryogenic detectors, thus reaching even more fields of research and further extending the outreach of the project.

An intercomparison exercise is currently ongoing among NMIs for the standardization of ^{109}Cd. The results will strengthen/broaden our calibration and measurement capability (CMC) claims for a multitude of methods of standardization. Ultimately standardised sources will be submitted to SIR resulting in updates of KCRV for derived SI units of Bq.

Availability of electron capture probabilities

The BetaShape code, which has been further developed within this project, has been used to provide electron capture probabilities (as well as beta spectra) for a major international collaboration on nuclear decay data evaluation: the Decay Data Evaluation Project (DDEP). This collaboration provides decay scheme data to the metrology community and a large audience of users, from fundamental physics to nuclear reactor industry and nuclear medicine. The entire DDEP database has been updated and the improved data have been made freely available at: http://www.lnhb.fr/nuclear-data/nuclear-data-table/. Executables of the BetaShape code have also been made freely available for various platforms at: http://www.lnhb.fr/rd-activities/spectrum-processing-software/.

Impact on relevant standards

The project has led to improved nuclear decay data by direct measurements and by improving the theoretical calculation techniques. Hence, the outcome of this project is a valuable contribution for nuclear decay data evaluations.

The SI derived unit of the becquerel must be established for each radionuclide individually and generally requires a multitude of primary standardisation methods for each radionuclide. For several pure EC nuclides, the TDCR-LSC method is the preferred method. Within the project, it was demonstrated that more precise EC probabilities had immediate impact on the corresponding activity standards and better knowledge of the electron and photon emission spectra and intensities will lead to further improvements when standardising EC radionuclides.

Longer-term economic, social and environmental impacts

This project has accelerated innovation and competitiveness in the field of the ground-breaking technology using MMCs and more generally cryogenic detectors. Other metrology institutes are already beginning to get involved in this field, which is certainly also a consequence of the success of this project and its predecessor MetroBeta. On a long-term perspective, MMC-based detectors may become a tool for enhanced nuclear spectrometry with an energy resolution which is much higher than with any semi-conductor detector. In particular, spectrometry at very low energy, where the detection efficiency of conventional techniques drastically drops off, benefits from the outstanding low energy threshold of MMCs, enabling substantial reduction of systematic effects. Ultimately MMC detectors enable research and applications far beyond current limits which are, at present, defined by existing spectrometers based on semi-conductors. Due to the high potential of MMCs, it is anticipated that the technology will be widely used in various disciplines. The nuclear decay data which has been determined with better precision beyond this project will be important in many fields such as nuclear medicine, industry or geo- and cosmochronology.

6 List of publications

1. Mougeot, X.: Towards high-precision calculation of electron capture decays. In: Applied Radiation and Isotopes 154 (2019), 108884, https://doi.org/10.1016/j.apradiso.2019.108884
2. Martins, L. et al.: Multiconfiguration Dirac-Fock calculations of Zn K-shell radiative and non radiative transitions. In: X-Ray Spectrometry 49, Issue 1 (2019), 192 – 199, https://doi.org/10.1002/xrs.3089
3. Martins, L. et al.: Overview and calculation of X-ray K-shell transition yields for comprehensive data libraries. In: X-Ray Spectrometry (2020), https://doi.org/10.1002/xrs.3123
4. Paulsen, M. et al.: Development of a Beta spectrometry setup using metallic magnetic calorimeters. In: Journal of Instrumentation 14 (2019), P08012, https://doi.org/10.1088/1748-0221/14/08/P08012
5. Bockhorn, L. et al.: Improved Source/ Absorber Preparation for Radionuclide Spectrometry Based on Low-Temperature Calorimetric Detectors. In: Journal of Low Temperature Physics (2019), https://doi.org/10.1007/s10909-019-02274-8
6. Fretwell, S. et al.: Direct Measurement of the ^{7}Be L/K Ratio in Ta-Based Superconducting Tunnel Junctions. In: Physical Review Letters 125, 032701 (2020), https://doi.org/10.1103/PhysRevLett.125.032701 and https://arxiv.org/abs/2003.04921v2
7. Ranitzsch, P. C.-O.: MetroMMC: Electron-Capture Spectrometry with Cryogenic Calorimeters for Science and Technology. In: Journal of Low Temperature Physics (2019), https://doi.org/10.1007/s10909-019-02278-4
8. Braß, M., Haverkort, M.W.: Ab initio calculation of the electron capture spectrum of Ho-163: Auger–Meitner decay into continuum states. In: New Journal of Physics 22, 093018 (2020), https://doi.org/10.1088/1367-2630/abac72
9. Hao, L. et al.: Coupled Resonator for Particle Detection. In: IEEE Transactions on Instrumentation & Measurement, 1006406, (2021), https://doi.org/10.1109/TIM.2021.3062171

10. Mougeot, X. et al.: Influence of the atomic modeling on the electron capture process. Submitted to Physical Review A (2021). Preprint available on arXiv: http://arxiv.org/abs/2111.15321

This list is also available here: https://www.euramet.org/repository/research-publications-repository-link/